



# Numerical investigations on the modelling of ultrafine particles in SSH-aerosol-v1.3a: size resolution and redistribution

Oscar Jacquot<sup>1</sup> and Karine Sartelet<sup>1</sup>

<sup>1</sup>CEREA, Ecole nationale des ponts et chaussées, EdF R&D, IPSL, Marne la Vallée, France

**Correspondence:** Oscar Jacquot (oscar.jacquot@enpc.fr) and Karine Sartelet (karine.sartelet@enpc.fr)

**Abstract.** As the health impact of ultrafine particles is getting better understood, modelling the size distribution and the number concentration with chemistry transport models becomes an increasingly important matter. The number concentrations is strongly affected by processes linked to aerosol dynamics: coagulation, condensation and gas/particle phase partitioning, nucleation. Coagulation is usually solved using an Eulerian approach, using a fixed diameter size discretization. In opposition, condensation/evaporation is rather solved using a Lagrangian approach, requiring redistribution of particles on the fixed grid size. Here, a new analytic formulation is presented to compute efficiently coagulation partition coefficients, allowing to dynamically adjust the discretization of the coagulation operator to the Lagrangian size mesh evolution, and therefore solve all the processes linked to aerosol dynamics with a Lagrangian approach, avoiding the redistribution on the fixed size grid. This new approach has the advantage of reducing the numerical diffusion introduced by condensation. The significance of these effects on number concentrations is assessed over Greater Paris with the chemistry transport model Polyphemus/Polair3D coupled to the aerosol model SSH-aerosol, using different size resolution of the particle distribution.

## 1 Introduction

As ultrafine particles, i.e. particles of diameters lower than  $0.1 \mu\text{m}$ , could exert different toxicity than larger particles (Ohlwein et al., 2019; Schraufnagel, 2020; Kwon et al., 2020) and represent an uncertain part in climate models (Forster et al., 2021), it is becoming increasingly important to represent them accurately in models from the indoor and local scale (Patel et al., 2021; Frohn et al., 2021) to the global scale (Leinonen et al., 2022). Those particles are characterized by low mass but high number concentrations. Therefore, integrated mass concentrations, such as  $\text{PM}_{10}$  and  $\text{PM}_{2.5}$ , bear little information about their significance. Chemistry-transport models (CTM) are frequently used to estimate pollutant concentrations, with applications from continental and regional scales, up to the urban scale. These models can be used to assess the impact of different emission scenarios, and they have long focus on representing the mass of particles of diameters lower than  $2.5 \mu\text{m}$  and  $10 \mu\text{m}$  ( $\text{PM}_{2.5}$  and  $\text{PM}_{10}$  respectively).

Different strategies have been developed to model the aerosol size distribution, among which the most common in CTMs are the sectional size distribution, which represent the distribution by piecewise approximations (e.g. Gelbard et al., 1980; Debry and Sportisse, 2007) and the modal approach, which represents the size distribution as a superposition of several modes, often log-normal ones (e.g. Whitby and McMurry, 1997; Vignati et al., 2004; Sartelet et al., 2006). Computationally competitive



and accurate numerical approaches are needed to represent both mass and number concentrations with a limited number of sections or modes. The modal approach is often favoured for its low computational requirements, while the sectional approach is favored for its numerical accuracy. For modelling aerosol mass concentrations, as little as three to ten sections are used (Pilinis and Seinfeld, 1988; Fast et al., 2006; Sartelet et al., 2018; Chang et al., 2021; Menut et al., 2021). However a higher  
30 number of sections may be required to simulate accurately particle number concentrations, as it is strongly influenced by size distribution. The number of sections used then typically range from twenty-five sections (Sartelet et al., 2022), 30 sections (Adams and Seinfeld, 2002) to 41 sections (Patoulias et al., 2018).

Aerosol dynamics involve multiple processes, which are associated to exchanges between and within phases (Warren and Seinfeld, 1985). Nucleation represents gas molecules forming a stable condensed aggregate (Laaksonen et al., 1999; Vehkamäki et al., 2002). Coagulation is associated to collision of particles, which leads to the formation of larger particles (v Smoluchowski, 1918). For atmospheric aerosols, Brownian motion is the main processes leading to coagulation (Fuchs, 1964). Condensation and evaporation are dual processes involving gas/particle phase partitioning governed by the gradient between the gas-phase concentration and the concentration at the surface of the particle. The Kelvin effect plays an important role on the evolution of ultrafine particles. It models the influence of the particle curvature, which increases the apparent saturation vapor  
40 pressure of chemical compounds (Thomson, 1871; Tolman, 1949), making the condensation of semi-volatile compounds more difficult and favouring their evaporation.

The condensation/evaporation process is formerly equivalent to advection in the space of aerosol volume. In that setting, the classical Lagrangian approach which aims at limiting numerical diffusion that would be introduced by the numerical discretization in an Eulerian frame of reference is therefore often applied (Neuman, 1984; Seigneur et al., 1986; Tsang and Rao,  
45 1988; Gelbard, 1990). This Lagrangian approach is however conflicting with the Eulerian one often used to solve the coagulation process, which involves interactions between different aerosol size ranges (Gelbard et al., 1980). Typically, because this process is usually treated in a Eulerian fashion, it requires a fixed discretization. To solve both coagulation and condensation/evaporation, models are required to switch between Lagrangian and Eulerian frameworks, introducing numerical diffusion which may hinder numerical performance.

An advantage of keeping a fixed discretization is to avoid rediscrretization of the coagulation operator, which would require computing partition coefficients. Indeed, the discretized equations describing the dynamics of aerosols by coagulation involve partition coefficients, which take into account the fact that the coagulation of particles from 2 size sections may lead to particle sizes that cover several sections. They are usually written as  $R_{jk}^i$ , which represents the fraction of coagulation between the sections  $j$  and  $k$  that ends up in section  $i$ . If the size discretization is fixed, these coefficients can be precalculated. Formulations  
55 of these coefficients, such as Jacobson et al. (2005), are based on heuristical considerations, without considering the wide range of diameters that may be encountered within a section. Other approaches (Debry and Sportisse, 2007; Dergaoui et al., 2013) are derived from assumptions on the underlying distribution of particles within each section. In (Dergaoui et al., 2013; Sartelet et al., 2020), partition coefficients are estimated numerically by a Monte Carlo “hit and miss” method. Although this method may be computationally expensive, it is easily generalised to simulate particle population of different mixing states. Here, an  
60 analytical expression is derived in the setting of uniformly distributed particles with each section.



Three dimensional chemistry-transport or global models represent the flow of air masses in an Eulerian manner (Sartelet et al., 2018; Menut et al., 2021; Appel et al., 2021). The sections or modes also need to be of distinct and fixed size ranges for numerical consistency throughout the simulations. In other words, as particles grow/shrink with condensation/evaporation in each grid cell, the bounds of the sections or modes evolve, and it is necessary to redistribute the number and mass or  
65 moments, introducing numerical errors and diffusion. Different strategies have been developed to mitigate issues arising in aerosol distribution representation. In the modal approach, modes can evolve freely over the whole size spectrum. However, modes may overlap due to aerosol dynamics, leading to numerical difficulties. Mode merging schemes have been developed to mitigate these difficulties, by merging modes that are overlapping (Whitby et al., 2002; Binkowski and Roselle, 2003). Mode merging may also be applied for each mode when the diameter of the distribution exceeds a fixed diameter (Sartelet  
70 et al., 2007). In the sectional approach, different algorithms can be used to redistribute sections onto a fixed grid. They usually conserve mass, e.g. the Euler method (Gelbard et al., 1980; Seigneur, 1982; Devilliers et al., 2013), the fixed sectional method (Gelbard, 1990; Karl et al., 2022), and often conserve both mass and number, e.g. the two-moment approach (Tzivion et al., 1987; Adams and Seinfeld, 2002) used in different aerosol models such as in MOZAIC (Fast et al., 2006) or the aerosol model included in the CTM PMCAMx (Patoulias et al., 2018); the moving diameter (Jacobson, 1997) used in MOZAIC (Fast et al.,  
75 2006), SIREAM (Debry and Sportisse, 2007), SSH-aerosol (Sartelet et al., 2020); the hybrid bin method (Chen and Lamb, 1994) used in SALSA (Kokkola et al., 2018); or the Euler-coupled algorithm (Devilleers et al., 2013) used in SSH-aerosol.

In order to evaluate the significance of errors introduced by numerical diffusion during the coupled integration of coagulation, condensation-evaporation and nucleation, a new algorithm coined 'Lagrangian aerosol dynamics' is proposed and implemented, making it possible to do away with the Eulerian approach to solve coagulation. To remain in a Lagrangian frame  
80 of reference, the representation of coagulation needs to be dynamically adapted to the size mesh evolution. The proposed algorithm, which avoids redistribution when solving aerosol dynamics, is presented in section 2. The chemistry-transport model used to assess the impact on concentrations and the setup of the 3D simulations are presented in section 3. Finally, the impact of different size resolutions and of the new algorithm are presented in section 4.

## 2 Lagrangian and Eulerian representation of aerosol processes

85 Using the sectional approach, the aerosol distribution is described using the number and mass densities integrated over different intervals. Let  $\{v_i\}_{i=0,m}$  a partitioning of the interval  $[v_0, v_{\max}]$  such that  $v_{i-1} < v_i$  with  $v$  the aerosol volume,  $n$  the aerosol number density and  $q_s$  the aerosol mass density of species  $s$ :

$$N_i(t) = \int_{v_{i-1}}^{v_i} dv n(v, t) \quad (1)$$

$$Q_{i,s}(t) = \int_{v_{i-1}}^{v_i} dv q_s(v, t) \quad (2)$$



90 The general dynamics equation represents the evolution of the aerosol density under the processes of coagulation, condensation-  
 evaporation and nucleation (Gelbard et al., 1980). Detailed expressions are recalled in Appendix A, and the discretized equa-  
 tions using the sectional approach in Appendix B.

## 2.1 Computation of partitioning coefficients

Partitioning coefficients emerge through the classical sectional approach. Assuming a piecewise constant distribution on each  
 95 interval provides a numerical closure for equations (A5) and (A6):

$$\begin{aligned} \frac{dN_i}{dt} = & \frac{1}{2} \sum_j \sum_k N_j N_k \iint dv du K(u, v-u) \mathbb{1}_{[v_{j-1}, v_j]}(u) \mathbb{1}_{[v_{k-1}, v_k]}(v-u) \\ & - \sum_k N_i N_k \iint dv du K(v, u) \mathbb{1}_{[v_{i-1}, v_i]}(v) \mathbb{1}_{[v_{k-1}, v_k]}(u) \end{aligned} \quad (3)$$

$$\begin{aligned} \frac{dQ_{i,s}}{dt} = & \sum_j \sum_k Q_j N_k \iint dv du K(u, v-u) \mathbb{1}_{[v_{j-1}, v_j]}(u) \mathbb{1}_{[v_{k-1}, v_k]}(v-u) \\ & - \sum_k Q_i N_k \iint dv du K(v, u) \mathbb{1}_{[v_{i-1}, v_i]}(v) \mathbb{1}_{[v_{k-1}, v_k]}(u) \end{aligned} \quad (4)$$

With the approximation that the kernel  $K$  can be factored out and estimated by an averaged quantity over each subdomain  
 $[v_{j-1}, v_j] \times [v_{k-1}, v_k]$ , it is possible to derive an algebraically closed form for the partitioning coefficients, which are only  
 100 functions of the chosen volume discretization. The double integration of piecewise constant functions leads to a piecewise  
 second-order polynomials, which only dependent on size (volume) mesh nodes:

$$R_{jk}^i = r_{jk}(v_i) - r_{jk}(v_{i-1}) \quad (5)$$

$$\begin{aligned} r_{jk}(v) = & \frac{1}{2} \frac{1}{v_j - v_{j-1}} \frac{1}{v_k - v_{k-1}} \times \left[ s\left(v - (v_{j-1} + v_{k-1})\right)^2 - s\left(v - (v_{j-1} + v_k)\right)^2 \right. \\ & \left. - s\left(v - (v_j + v_{k-1})\right)^2 + s\left(v - (v_j + v_k)\right)^2 \right] \end{aligned} \quad (6)$$

105 with  $s$  the ramp function, defined such that  $s(v) = 0$  if  $v < 0$  and  $s(v) = v$  if  $v \geq 0$ . We refer to Appendix C for a derivation of  
 this result, and to Appendix D for an equivalent expression, less compactly written but less sensitive to numerical truncation  
 errors due to subtractions of large numbers of similar order of magnitude. Note that a similar approach as the one derived  
 here was followed by Debry and Sportisse (2007) to estimate partition coefficients, but a mistake led to an inaccurate reported  
 closed form. This expression was implemented in the software SSH-aerosol, and its validity checked by comparison to a  
 110 coagulation test case defined in the software (Sartelet et al., 2020) that involves partition coefficients calculated with a Monte-  
 Carlo approach.



## 2.2 Lagrangian vs Eulerian formulation of aerosol dynamics

To solve the equations describing aerosol dynamics, the SSH-aerosol model (Sartelet et al., 2020) is used here. Coagulation, nucleation, condensation of extremely-low volatile organic and non-volatile compounds are solved simultaneously. The condensation/evaporation of semi-volatile aerosols is modelled using either a dynamic or a bulk equilibrium approach, assuming instantaneous thermodynamic equilibrium between the gas and bulk-aerosol phases. In the bulk approach, the size-section weighting factors depend on the ratio of the mass transfer rate in the aerosol distribution; and the Kelvin effect, which limits the condensation of those compounds on ultrafine particles, is modelled following Zhu et al. (2016). An explicit time-stepping algorithm (explicit trapezoidal rule) with adaptive time steps is used. After each time step, as the diameters of particles may have evolved because of the Lagrangian formulation of condensation, a redistribution scheme is applied, such as the moving diameter (Jacobson, 1997) or the Euler-coupled scheme (Devilleers et al., 2013). The outline of this implementation is described in Algorithm 1. To estimate the impact of redistributing every time step onto the fixed Eulerian grid, a Lagrangian algorithm is setup for aerosol dynamics, as described in 2. Partition coagulation coefficients are computed every time step, allowing for the size mesh to evolve. Note that redistribution is always performed at the end of a global time step  $t_{\text{final}}$ , which corresponds to the time step of the 3D-model.

---

### Algorithm 1 Lagrangian integration of condensation and Eulerian integration of coagulation

---

Compute coagulation partition coefficients

**while**  $t < t_{\text{final}}$  **do**

    Compute number and mass concentration evolution due to coagulation, condensation/evaporation and nucleation

    Redistribute number and mass concentrations on the fixed Eulerian grid

**end while**

---

---

### Algorithm 2 Lagrangian integration of condensation and coagulation

---

**while**  $t < t_{\text{final}}$  **do**

    Compute coagulation partition coefficients based on current size mesh

    Compute number and mass concentration evolution due to coagulation, condensation/evaporation and nucleation

**if** Some mesh size nodes have crossed **then**

        Redistribute number and mass concentrations on the fixed Eulerian grid

**end if**

**end while**

Redistribute number and mass concentrations on the fixed Eulerian grid

---



### 3 Chemistry-transport modelling

To evaluate the impact of solving aerosol dynamics with a Lagrangian approach and different numbers of sections, simulations are performed over Greater Paris with the two algorithms previously described.

#### 3.1 Numerical simulation setup

130 Numerical simulations are performed over the Greater Paris area using the Polyphemus/Polair3D (Mallet et al., 2007; Sartelet et al., 2018) chemistry-transport model coupled to the SSH-aerosol chemistry and aerosol dynamics model (Sartelet et al., 2020). For the reference simulation, a period of 12 days starting from 29 June 2009 is considered. The spatial resolution is  $0.02^\circ \times 0.02^\circ$ , and the setup is the same as in (Sartelet et al., 2022). The processes related to aerosol dynamics are solved after the processes related to transport and gaseous chemistry, with a splitting time step of 100 s. It means that redistribution of the  
135 fixed Eulerian grid is performed every 100 s regardless of the algorithm used for aerosol dynamics (Lagrangian vs Eulerian). For aerosol-related processes, coagulation, condensation, evaporation, and heteromolecular nucleation are considered. Heteromolecular nucleation involves sulfuric acid and extremely low volatile compounds, which are formed from autoxidation of terpenes (Riccobono et al., 2014).

In order to investigate model sensitivity to size resolution, aerosol concentrations are simulated with three different particle  
140 size discretization, ranging from 1 nm to  $10 \mu\text{m}$ . The finest discretization is made of 25 sections, the intermediate one of 14 sections, and the coarsest one of 9 sections. Section boundaries are defined similarly as in the study conducted by Sartelet et al. (2022) with geometrically uniform spacing below  $1 \mu\text{m}$ . All discretization are identical between  $1 \mu\text{m}$  and  $10 \mu\text{m}$ . Figure 1 depicts the discretizations considered in this study: 2, 4 and 8 sections are below 10 nm in the discretization with 9, 14 and 25 sections respectively, 2, 4 and 8 sections are respectively in the range 10-160 nm, and 2, 3 and 6 sections are between 160 nm  
145 and  $1 \mu\text{m}$ .

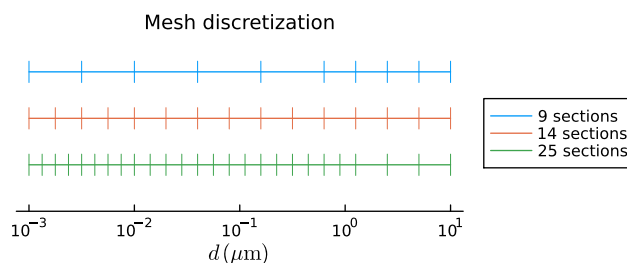


**Figure 1.** Considered discretization for each mesh

The redistribution method used is the Euler-Coupled algorithm (Devilliers et al., 2013). For 25 sections, emissions and boundary conditions are the same as in Sartelet et al. (2022). The consistency of these forcings across all size resolutions has been ensured by maintaining both mass and number across resolutions.



### 3.2 Comparison to observations

150 To assess the validity of the model, comparisons between observations and simulated concentrations are reported. Daily number concentration of particles of diameter larger than 10 nm ( $N_{>10}$ ) are compared to measurements at two observation sites: LHVP (48.8°, 2.36°) representative of urban background concentrations, and the SIRTA observatory (48.7°, 2.21°) a suburban observation site. Multiple statistical indicators are provided in Table 1: the Normalised Mean Error (NME), the Normalised Mean Bias (NMB) and the fraction of modelled data within a factor of 2 of observations (FAC2). The NME and NMB are  
155 similar to those presented in Sartelet et al. (2022), and they are on the low side of those simulated elsewhere (Patoulias et al., 2018; Fanourgakis et al., 2019; Frohn et al., 2021; Olin et al., 2022). The FAC2 is higher than 50% for all simulations for  $N_{>10}$ , meeting the strictest model evaluation criterion defined in Chang and Hanna (2004). Simulations with 9, 14 and 25 sections display similar statistics for  $N_{>10}$ . The statistics are very similar between 9, 14 and 25 sections for  $N_{>10}$ , although the bias NMB is higher at LHVP with 9 sections. Statistics using the full-Lagrangian algorithm are not shown, as they are very  
160 similar to those of Table 1. The simulated concentrations of  $PM_{2.5}$  compare very well to the measurements, and the statistics for model to measurement comparisons of  $PM_{2.5}$  are very similar between the simulations with 9, 14 and 25 sections, as shown in Table 2. The number concentrations simulated with 25 sections and the Lagrangian algorithm are shown in Fig. 3. As previously discussed in Sartelet et al. (2022), the concentrations are higher in Paris than in the suburbs.

**Table 1.** Comparison of simulated and measured daily number concentrations of particles  $N_{>10}$  between 29 June and 10 July 2009, at the observation sites LHVP and SIRTA. Mean observed ( $\bar{o}$ ) and mean simulated ( $\bar{s}$ ) daily number concentrations are reported in  $\#.cm^{-3}$ . Fraction of modelled data within a factor of 2 of observations (FAC2) as well as normalized mean bias (NMB) and normalized mean error (NME) are reported in %.

	SIRTA					LHVP				
	$\bar{o}$	$\bar{s}$	FAC2	NMB	NME	$\bar{o}$	$\bar{s}$	FAC2	NMB	NME
9 sections	5215	4806	62	-8	35	8804	7045	99	-20	30
14 sections	5215	5463	92	10	35	8804	8144	99	-7	28
25 sections	5215	5422	92	9	35	8804	8225	99	-7	28

### 4 Influence of the size resolution and redistribution

165 Model output sensitivity to numerical diffusion is estimated by comparing the Lagrangian algorithm to the standard Eulerian one, where condensation/evaporation is performed in a Lagrangian manner and projected back on the Eulerian grid. The sensitivity to the grid resolution is also studied, and provides valuable information about the ability to reduce numerical diffusion by increasing resolution in an Eulerian setting, as well as an estimation of the relative magnitude of numerical errors associated to numerical diffusion and other error sources.

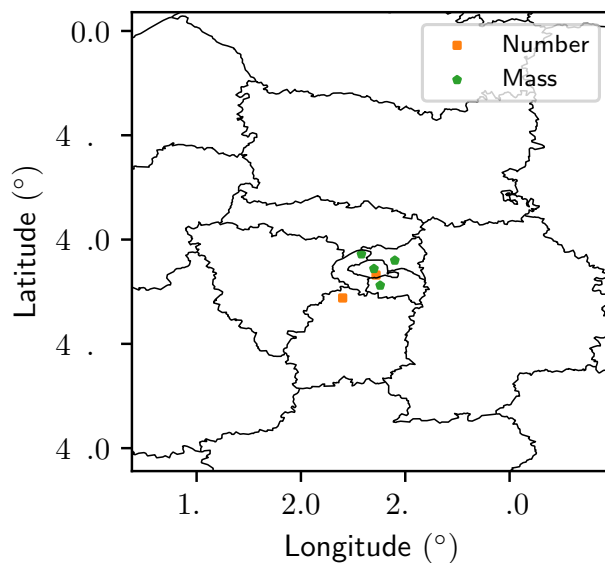


**Figure 2.** Location of observation sites, for reported number and mass measurements.

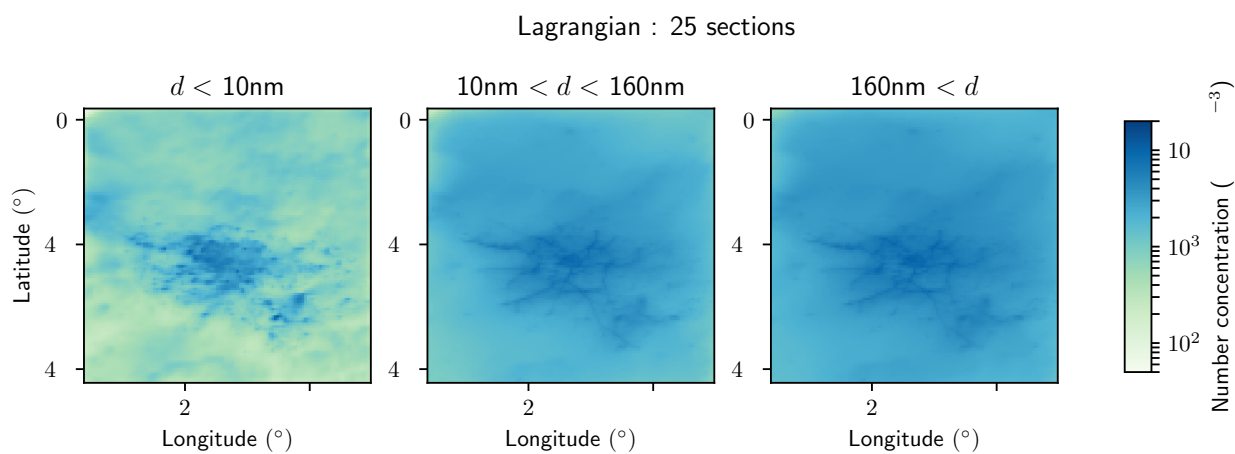


**Figure 3.** Aerosol number concentrations simulated with 25 sections and the Lagrangian algorithm





**Table 2.** Comparison of simulated and measured daily  $\text{PM}_{2.5}$  concentrations between 29 June and 10 July 2009, at four available measurement stations available from the AIRPARIF network. Mean observed ( $\bar{o}$ ) and mean simulated ( $\bar{s}$ ) daily mass concentrations are reported in  $\mu\text{g}\cdot\text{m}^{-3}$ . Fraction of modelled data within a factor of 2 of observations (FAC2) as well as normalized mean bias (NMB) and normalized mean error (NME) are reported in %.

	$\bar{o}$	$\bar{s}$	FAC2	NMB	NME
9 sections	10.4	8.5	94	-12	32
14 sections	10.4	8.7	94	-11	31
25 sections	10.4	8.9	94	-10	30

#### 170 4.1 Sensitivity to numerical diffusion

The simulations using the Eulerian and Lagrangian algorithms are compared using either 9, 14 or 25 sections in Fig. 4, 5 and 6 respectively, and time-space averages are compiled in Table 3. The comparison is performed for the number of particles of diameters lower than 10 nm ( $N_{<10}$ ), between 10 nm and 160 nm ( $N_{10-160}$ ), and higher than 160 nm ( $N_{>160}$ ). For each size resolution considered, average relative differences between the number concentrations simulated with both algorithms are  
175 higher for particles of smaller diameters: they are higher for  $N_{<10}$  than for  $N_{10-160}$  than for  $N_{>160}$ . This is consistent with the expected properties of particles, as small particles are more influenced by aerosol dynamics and evolve more quickly than large particles. They are therefore the one most susceptible to numerical diffusion.

With 9 and 14 sections, the average relative differences for  $N_{<10}$  between simulations using the Eulerian and Lagrangian algorithms are about 16% and 5% respectively (Table 3). They can be much higher locally, reaching 20% (Fig. 4 and 5),  
180 although the largest differences are observed where the number concentrations are lowest (Fig. 3). Relative differences are more smoothly spatially distributed for larger particles, with relative differences staying below a few percents. The total number of particles with a diameter higher than 160 nm is much less sensitive to the choice of algorithm, with relative differences around 2 to 3% on average.

At higher resolution, with 25 sections, the same general trends are observed (Table 3). While  $N_{<10}$  concentrations are more  
185 sensitive to the choice of the algorithm than those of particles with higher diameters, the relative error is contained under 10% globally (Figure 3), and at 3.3% on average. Compared to 9 and 14 sections, concentrations are less sensitive to the choice of the algorithm. This is an expected behavior, as higher resolution Eulerian schemes are themselves less diffusive. At all resolution, the sensitivity of  $N_{>10}$  to the choice of the algorithm is limited: 2.6% in average for 14 and 25 sections, and 3.5% for 9 sections.

#### 190 4.2 Sensitivity to size resolution

To put into perspective the relative differences observed between the numerical algorithms, comparison is performed between the three different resolutions (9, 14 and 25 size sections). Relative differences between number concentrations for different



**Table 3.** Average relative differences between simulations using the Eulerian and Lagrangian algorithms, for aerosol number concentrations. Averages are estimated over all timesteps and spatial gridpoints.

Resolution	Average relative difference (%)			
	$d < 10$ nm	$10 \text{ nm} < d < 160$ nm	$160 \text{ nm} < d$	$10 \text{ nm} < d$
9 sections	15.8	4.9	2.5	3.5
14 sections	5.4	3.5	2.0	2.6
25 sections	3.3	3.2	2.2	2.6

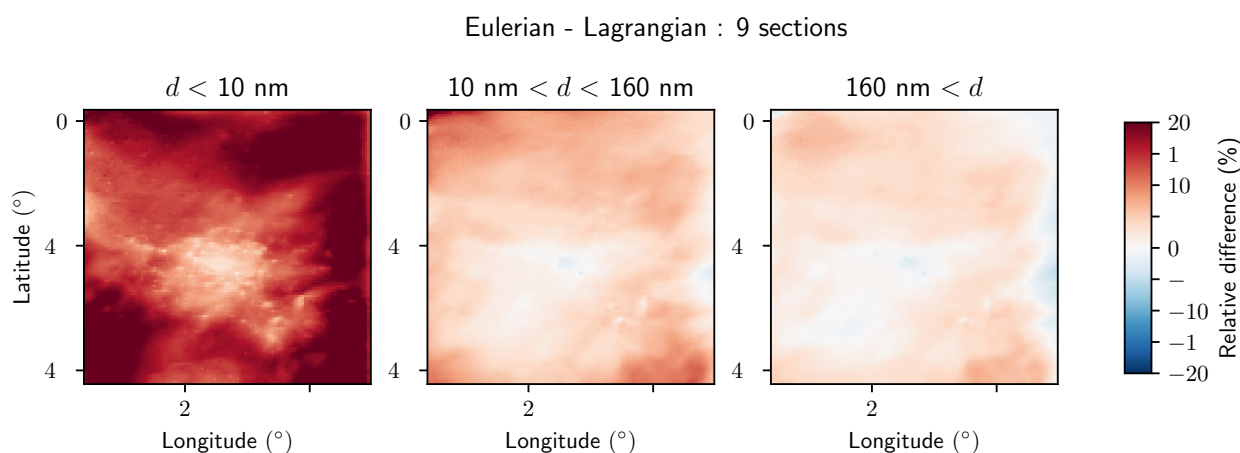


**Figure 4.** Relative difference between number concentrations simulated with the Eulerian and Lagrangian algorithms, using 9 sections.

particle diameter ranges simulated with 9 and 14 sections, using 25 sections as a reference, are displayed in Fig. 7 and 8 respectively.

195 Globally, the sensitivity to the size resolution is higher than the sensitivity to the choice of the aerosol dynamics algorithm. The  $N_{<10}$  concentrations display significant variability, with average relative differences of the order of 300% for 9 sections, and 50% for 14 sections (Table 4). The sensitivity to the size resolution is lower for number concentrations of particles of higher diameters ( $N_{10-160}$  and  $N_{>160}$ ). For  $N_{>10}$ , the average difference between 14 and 25 sections is low (about 2.3%), but the difference between 9 and 25 sections is much higher (22%). As for the evaluation of the sensitivity to the aerosol dynamics  
 200 algorithm, spatial inhomogeneities are larger for smaller particles ( $N_{<10}$ ). The sensitivity to the size resolution is very similar for both schemes (Table 4). Additional figures describing the sensitivity to the size resolution using the Lagrangian algorithm are shown in Appendix E.

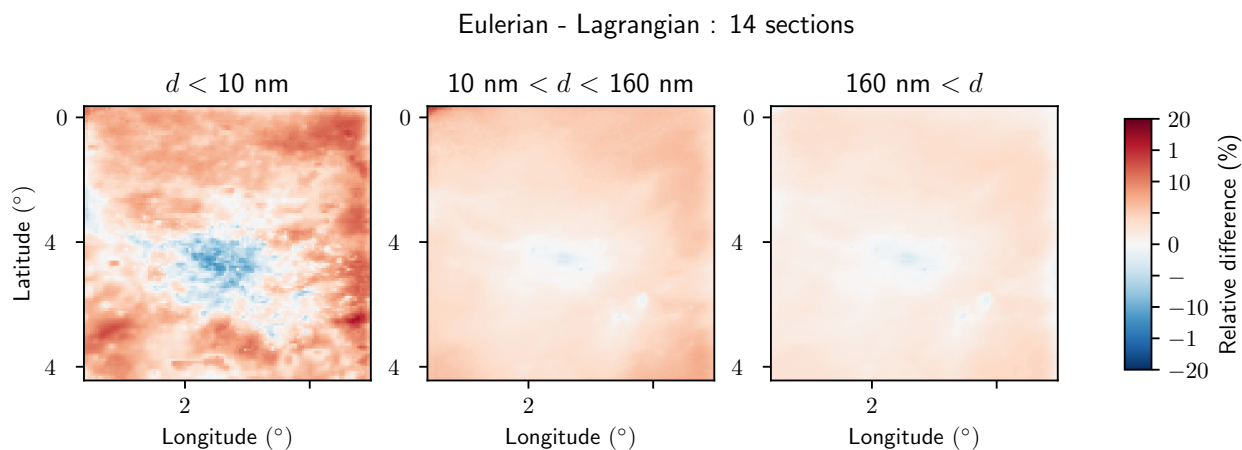


**Figure 5.** Relative difference between number concentrations simulated with the Eulerian and Lagrangian algorithms, using 14 sections.

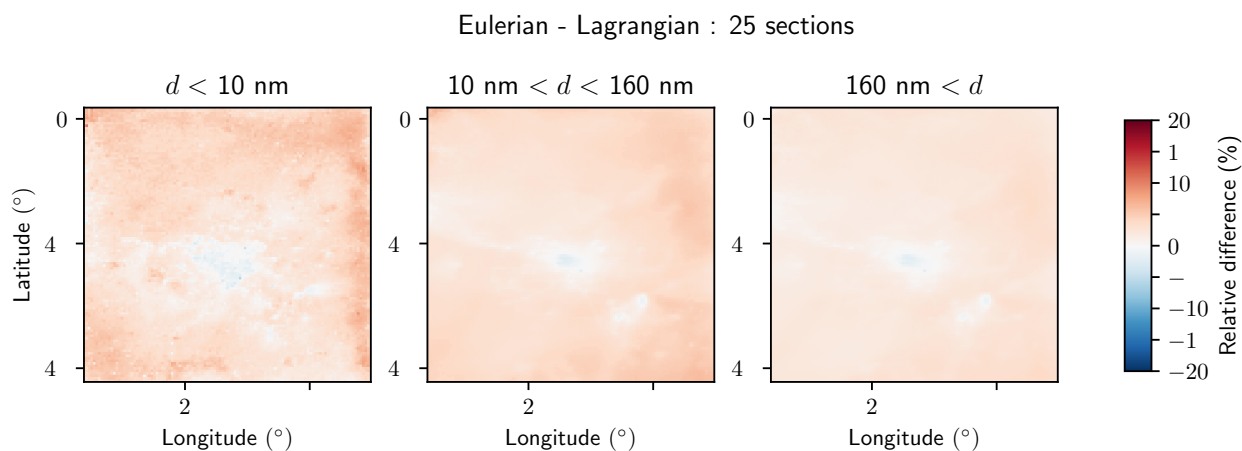


**Figure 6.** Relative difference number concentrations simulated with the Eulerian and Lagrangian algorithms, using 25 sections.

## 5 Conclusions

A new algorithm that enables coupled integration of aerosol condensation, evaporation nucleation and coagulation in a Lagrangian framework has been introduced. This algorithm is an extension of classical schemes for which the coagulation operator is dynamically updated to match the size mesh evolution under the condensation-evaporation process. The main advantage of this scheme is to limit numerical diffusion during the resolution of aerosol dynamics.



**Table 4.** Average relative differences between simulations with 14 and 25 size sections, using either the Eulerian or the Lagrangian algorithms, for aerosol number concentration. The average is estimated over all timesteps and spatial gridpoints.

		Average relative difference (%) compared to 25 sections			
Resolution	Algorithm	$d < 10$ nm	$10 \text{ nm} < d < 160$ nm	$160 \text{ nm} < d$	$10 \text{ nm} < d$
9 sections	Eulerian	336.3	15.5	27.3	22.0
	Lagrangian	288.7	16.6	27.4	22.6
14 sections	Eulerian	51.8	10.2	5.0	2.3
	Lagrangian	49.9	10.0	4.7	2.5

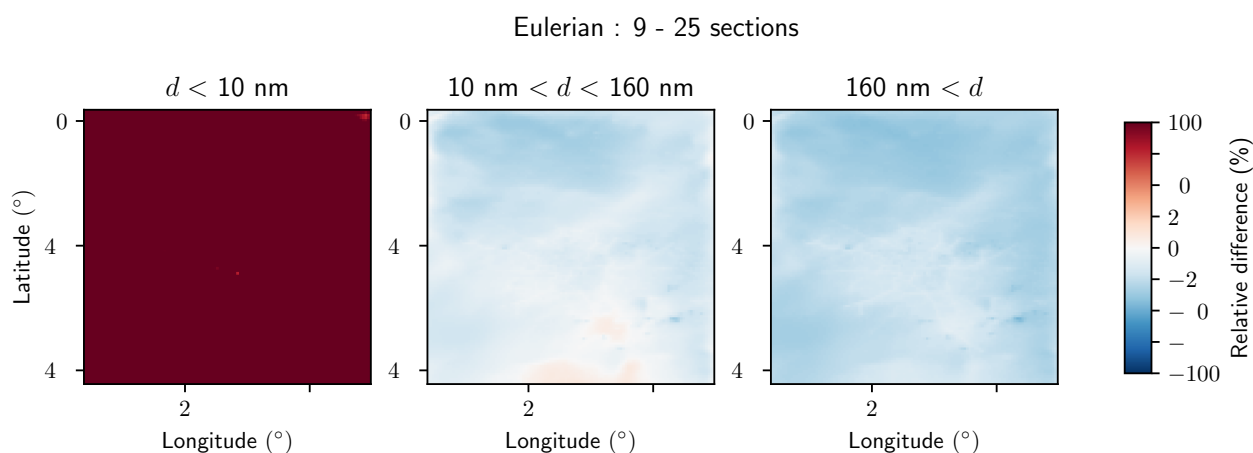


**Figure 7.** Relative differences between number concentrations for different particle diameter ranges, simulated with 9 and 25 sections. The Eulerian algorithm is used.

The impact of this algorithm on the number concentrations simulated over Greater Paris was investigated with the chemistry transport model Polyphemus/Polair3D. The number concentrations of particles of diameters below 10 nm are more impacted than larger particles, as these small particles are more subject to processes linked to aerosol dynamics. The impact of the Lagrangian algorithm decreases as the size resolution increases. It is higher when 9 size sections are used to discretize the ranges of diameters, than when 14 or 25 sections are used. For particles of diameters below 10 nm, the average relative difference between concentrations simulated using the Lagrangian and Eulerian algorithms is about 16% with 9 sections, but only 5% with 14 sections and 3% with 25 sections. As the use of the Lagrangian algorithm results in additional computation time, it is more relevant at low resolutions as higher benefits are then expected.

Number concentrations are more sensitive to the size resolution than to the aerosol dynamics algorithm, especially for the number of particles below 10 nm, indicating that averaging over wide size ranges is a limiting factor. The average differences of number concentrations for particles of diameter higher than 10 nm, computed with the finest resolution simulation as a

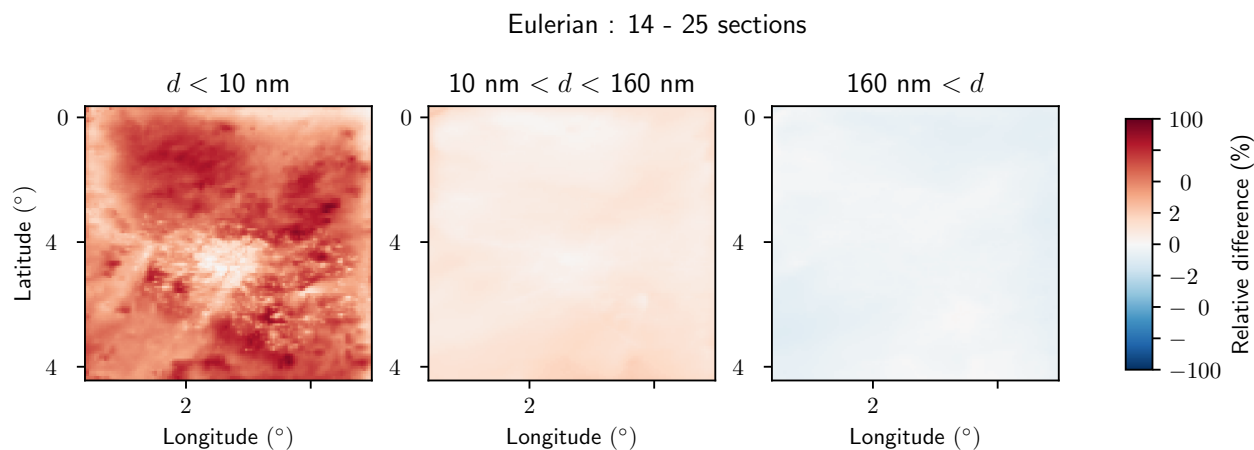


**Figure 8.** Relative differences between number concentrations for different particle diameter ranges, simulated with 14 and 25 sections. The Eulerian algorithm is used.

reference, are of the order of magnitude of 20 % using 9 sections and 2 % using 14 sections. Both simulated  $\text{PM}_{2.5}$  and  $N_{>10}$  concentrations compare well to observations for 9, 14 and 25 sections. However, the bias of  $N_{>10}$  concentrations compared to measurements is noticeably higher in the station in Central Paris for 9 than for 14 and 25 sections (-20% against -7%). Hence, 14 sections is recommended as a good compromise between complexity and performance.

This paper has focused on modelling number concentrations with an Eulerian chemistry-transport model, requiring, for 3D consistency, regular redistribution on a fixed size mesh. The new algorithm proposed was studied in the setting of 3D CTM with Eulerian transport of air masses, however it may present a greater impact using 3D Lagrangian models, which deal with advection in physical space in a Lagrangian fashion (Pandis et al., 1992; Fast et al., 2012). For those types of models, regular redistribution on a fixed size grid is not needed. Therefore, one could foresee that numerical diffusion associated to the resolution of aerosol dynamics would then be the dominant source of numerical diffusion.

*Code availability.* The software code for Polyphemus/Polair3D using SSH-aerosol with Eulerian or Lagrangian coagulation is available at <https://zenodo.org/doi/10.5281/zenodo.13135701>, as well as the scripts to compute the statistics and graphs. The software SSH-aerosol, Polyphemus and its dependencies are distributed under the GNU General Public License v3.

## Appendix A: General dynamics equation

Let  $v$  be the aerosol volume,  $n$  the aerosol number density and  $q_s$  the aerosol mass density of species  $s$ . Under classical internal mixing assumption, which considers that aerosols of a given size are of similar chemical composition, and accounting for



235 coagulation (coag.), condensation-evaporation (c/e) and nucleation (nucl), the evolution of the aerosol density is provided by the equation

$$\frac{\partial n}{\partial t}(v, t) = \frac{\partial n}{\partial t} \Big|_{c/e}(v, t) + \frac{\partial n}{\partial t} \Big|_{\text{coag.}}(v, t) + \frac{\partial n}{\partial t} \Big|_{\text{nucl.}}(v, t) \quad (\text{A1})$$

$$\frac{\partial q_s}{\partial t}(v, t) = \frac{\partial q_s}{\partial t} \Big|_{c/e}(v, t) + \frac{\partial q_s}{\partial t} \Big|_{\text{coag.}}(v, t) + \frac{\partial q_s}{\partial t} \Big|_{\text{nucl.}}(v, t) \quad (\text{A2})$$

with

$$240 \quad \frac{\partial n}{\partial t} \Big|_{c/e}(v, t) = -\frac{\partial}{\partial v}(I_0 n) \quad (\text{A3})$$

$$\frac{\partial q_s}{\partial t} \Big|_{c/e}(v, t) = -\frac{\partial}{\partial v}(I_0 q_s) + I_s n \quad (\text{A4})$$

$$\frac{\partial n}{\partial t} \Big|_{\text{coag.}}(v, t) = \frac{1}{2} \int_{v_0}^v du K(u, v-u) n(u, t) n(v-u, t) - n(v, t) \int_{v_0}^{v_{\max}} du K(v, u) n(u, t) \quad (\text{A5})$$

$$\frac{\partial q_s}{\partial t} \Big|_{\text{coag.}}(v, t) = \int_{v_0}^v du K(u, v-u) q_s(u, t) n(v-u, t) - q_s(v, t) \int_{v_0}^{v_{\max}} du K(v, u) n(u, t) \quad (\text{A6})$$

245 and

$$\frac{\partial n}{\partial t} \Big|_{\text{nucl.}}(v, t) = \delta(v - v_0) J_0(t) \quad (\text{A7})$$

$$\frac{\partial q_s}{\partial t} \Big|_{\text{nucl.}}(v, t) = \delta(v - v_0) J_0(t) m_s \quad (\text{A8})$$

where  $v_0$  is the volume of the smallest condensed aerosol aggregate,  $I_s$  is the volume growth rate related to condensation-evaporation for each species  $s$ ,  $I_0 = \sum_s I_s$  the total volume growth rate,  $K$  is the coagulation kernel,  $J_0$  the nucleation rate  
 250 involving the mass  $m_s$  of species  $s$  involved in the nucleation, and  $\delta$  is the Dirac distribution.

## Appendix B: Discretized aerosol dynamics

For coagulation, the time evolution of mass and number concentrations may be written as

$$\frac{dN_i}{dt} = \frac{1}{2} \sum_j \sum_k R_{jk}^i K_{jk} N_j N_k - N_i \sum_k K_{ik} N_k \quad (\text{B1})$$

$$\frac{dQ_i^s}{dt} = \sum_j \sum_k R_{jk}^i K_{jk} Q_j^s N_k - Q_i^s \sum_k K_{ik} N_k \quad (\text{B2})$$

255 where  $K_{jk}$  is the coagulation kernel associated to collision of particles from section  $j$  and  $k$ , and  $R_{jk}^i$  is the partition coefficient, associated to particle gains in section  $i$  from collisions of particles originating from sections  $j$  and  $k$ . The coagulation kernel is



modelled following Fuchs (1964), allowing to represent particles from the free molecular regime to the continuum one. A new and accurate algorithm to derive partitions coefficients is detailed in Section 2.1.

For condensation/evaporation and nucleation, the time evolution of mass and number concentrations may be written as

$$260 \quad \frac{dN_i}{dt} = J_s \delta_{i,1} \quad (\text{B3})$$

$$\frac{dQ_i^s}{dt} = 2\pi D_g d_p f(Kn_s, \alpha_s) \left[ C_g^s - C_a^s \exp\left(\frac{4\sigma_s v_s}{RT d_p}\right) \right] + J_0 \frac{\pi}{6} d_p^3 \rho_p \delta_{i,1} \quad (\text{B4})$$

with  $J_0$  the nucleation rate,  $d_p$  and  $\rho_p$  the particle wet diameter and density,  $D_g$  and  $C_g^s$  the molecular diffusivity in the air and the gas-phase concentration of species  $s$ ,  $f$  the Fuchs-Sutugin function, which depends on the Knudsen number of species  $s$  ( $Kn_s$ ) and on the accommodation coefficient  $\alpha_s$ ,  $C_a^s$  is the concentration at the particle surface assumed to be at local thermodynamic equilibrium with the particle composition,  $\sigma_s$  and  $v_s$  are the surface tension of species and molecular volume of species  $s$ .

### Appendix C: Partition coefficients for coagulation gains: closed form

Let  $R_{jk}^i$  denote the fraction of particles of volume contained between  $v_{i-1}$  and  $v_i$ , resulting from collisions of particles from sections  $j$  and  $k$ :

$$270 \quad R_{jk}^i = \int_{v_{i-1}}^{v_i} du (f_j * f_k)(u) \quad (\text{C1})$$

with  $*$  denoting the convolution product. Assuming uniform distribution within sections, we also have

$$f_j(v) = \frac{H(v - v_{j-1}) - H(v - v_j)}{v_j - v_{j-1}} \quad (\text{C2})$$

$$f_k(v) = \frac{H(v - v_{k-1}) - H(v - v_k)}{v_k - v_{k-1}} \quad (\text{C3})$$

with  $H$  the Heaviside step function.



275 To derive a closed form for Eq. (C1), let first compute the derivative of the convolution product

$$\begin{aligned}
 \frac{d}{dv}(f_j * f_k) &= f_j * \frac{df_k}{dv} \\
 &= f_j * \left[ \frac{1}{v_k - v_{k-1}} (\delta(u - v_{k-1}) - \delta(u - v_k)) \right] \\
 &= \frac{1}{v_k - v_{k-1}} [f_j * \delta(u - v_{k-1}) - f_j * \delta(u - v_k)] \\
 &= \frac{1}{v_k - v_{k-1}} [f_j(u - v_{k-1}) - f_j(u - v_k)] \\
 280 \quad &= \frac{1}{v_j - v_{j-1}} \frac{1}{v_k - v_{k-1}} \left[ H(v - (v_{j-1} + v_{k-1})) - H(v - (v_j + v_{k-1})) \right. \\
 &\quad \left. - H(v - (v_{j-1} + v_k)) + H(v - (v_j + v_k)) \right] \tag{C4}
 \end{aligned}$$

We can then derive  $f_j * f_k$  up to a constant  $\kappa$

$$\begin{aligned}
 (f_j * f_k)(v) + \kappa &= \int^v du \frac{d}{du}(f_j * f_k) \\
 285 \quad &= \frac{1}{v_j - v_{j-1}} \frac{1}{v_k - v_{k-1}} \int^v du \left[ H(u - (v_{j-1} + v_{k-1})) - H(u - (v_j + v_{k-1})) \right. \\
 &\quad \left. - H(u - (v_{j-1} + v_k)) + H(u - (v_j + v_k)) \right] \\
 &= \frac{1}{v_j - v_{j-1}} \frac{1}{v_k - v_{k-1}} \left[ s(v - (v_{j-1} + v_{k-1})) - s(v - (v_j + v_{k-1})) \right. \\
 &\quad \left. - s(v - (v_{j-1} + v_k)) + s(v - (v_j + v_k)) \right]. \tag{C5}
 \end{aligned}$$

As all terms are null at  $v = 0$ ,  $\kappa = 0$ .

290 Finally, a closed form for Eq. (C1) may be written as:

$$R_{jk}^i = \int_{v_{i-1}}^{v_i} du (f_j * f_k)(u) = r_{jk}(v_i) - r_{jk}(v_{i-1}) \tag{C6}$$

with  $r_{jk}$  a primitive of  $f_j * f_k$

$$\begin{aligned}
 r_{jk}(v) &= \frac{1}{2} \frac{1}{v_j - v_{j-1}} \frac{1}{v_k - v_{k-1}} \times \left[ s(v - (v_{j-1} + v_{k-1}))^2 - s(v - (v_{j-1} + v_k))^2 \right. \\
 &\quad \left. - s(v - (v_j + v_{k-1}))^2 + s(v - (v_j + v_k))^2 \right] \tag{C7}
 \end{aligned}$$

#### Appendix D: Closed form with improved numerical stability

295 The closed form derived in Appendix C is analytically exact, but a direct numerical implementation under this form would lead to imprecise results do to a large sensitivity to numerical truncature under this form. For instance, if we take  $v > v_j + v_k$ ,





all terms simplify to 1. However, a naive numerical approach would compute the square of all differences between  $v$  and quantities such as  $v_j + v_k$ . In this setting, we would then subtract numbers of similar magnitude, and possibly introduce significant rounding errors. The global form proposed in Appendix C is advantageous to simplify its derivation, but equivalent and more stable form exist. Therefore, a different form is proposed for numerical evaluation, where analytically equivalent forms are employed on different subintervals of the whole domain, improving numerical accuracy.

Let us define  $\Delta v_j = v_j - v_{j-1}$  and  $\Delta v_k = v_k - v_{k-1}$ . Without loss of generality let us assume that  $\Delta v_j > \Delta v_k$ , up to a permutation. Let us define

$$\alpha_{jk} = v_{j-1} + v_{k-1} \quad (D1)$$

$$305 \quad \beta_{jk} = v_{j-1} + v_k \quad (D2)$$

$$\gamma_{jk} = v_j + v_{k-1} \quad (D3)$$

$$\delta_{jk} = v_j + v_k. \quad (D4)$$

These new variables are in increasing order  $\alpha_{jk} < \beta_{jk} < \gamma_{jk} < \delta_{jk}$ , and can be introduced in Equation (C7)

$$r_{jk}(v) = \frac{1}{2} \frac{1}{\Delta v_j \Delta v_k} [s(v - \alpha_{jk})^2 - s(v - \beta_{jk})^2 - s(v - \gamma_{jk})^2 + s(v - \delta_{jk})^2] \quad (D5)$$

310 Each interval defined by the partition of  $[v_0, \infty]$  at points  $\alpha_{jk}, \beta_{jk}, \gamma_{jk}, \delta_{jk}$  has an increasing amount of non-zero terms in this expression. Simplification between terms occur when considering the restriction to each of these subintervals.

$$\begin{cases} r_{jk}(v) = 0 & \text{if } v < \alpha_{jk} \\ r_{jk}(v) = \frac{1}{2} \frac{1}{\Delta v_j \Delta v_k} (v - \alpha_{jk})^2 & \text{if } \alpha_{jk} < v < \beta_{jk} \\ r_{jk}(v) = \frac{1}{2} \frac{\Delta v_k}{\Delta v_j} + \frac{v - \beta_{jk}}{\Delta v_j} & \text{if } \beta_{jk} < v < \gamma_{jk} \\ r_{jk}(v) = 1 - \frac{1}{2} \frac{1}{\Delta v_j \Delta v_k} (v - \delta_{jk})^2 & \text{if } \gamma_{jk} < v < \delta_{jk} \\ r_{jk}(v) = 1 & \text{if } v < \delta_{jk} \end{cases} \quad (D6)$$

## Appendix E: Additional figures

315 *Author contributions.* KS and OJ participated to the conceptualization of the study. OJ set up the equations determining the partition coefficients. OJ and KS implemented the new scheme. KS performed the 3D numerical simulations and the model evaluation. KS and OJ conducted the visualization and wrote the manuscript.

*Competing interests.* The authors declare no competing interests.

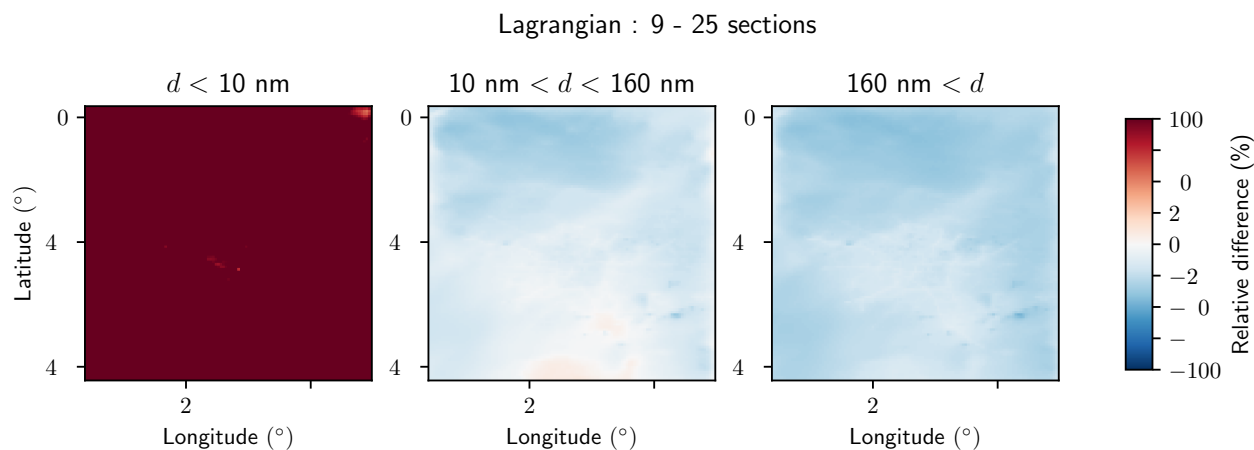


**Figure E1.** Relative difference between number concentrations for different particle diameter ranges, simulated with the coarse (9 sections) and fine discretisation (25 sections), using the Lagrangian algorithm.

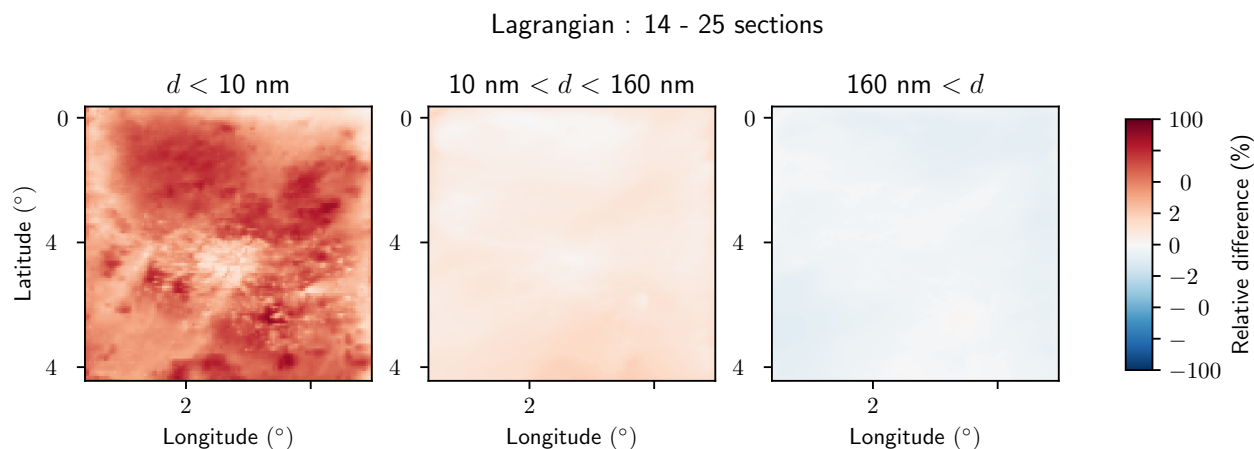


**Figure E2.** Relative difference between number concentrations for different particle diameter ranges, simulated with the medium (14 sections) and fine discretisation (25 sections), using the Lagrangian algorithm.

## References

- Adams, P. J. and Seinfeld, J. H.: Predicting Global Aerosol Size Distributions in General Circulation Models, *J. Geophys. Res. Atmos.*, 107, AAC 4–1–AAC 4–23, <https://doi.org/10.1029/2001JD001010>, 2002.
- Appel, K. W., Bash, J. O., Fahey, K. M., Foley, K. M., Gilliam, R. C., Hogrefe, C., Hutzell, W. T., Kang, D., Mathur, R., Murphy, B. N., Napelenok, S. L., Nolte, C. G., Pleim, J. E., Pouliot, G. A., Pye, H. O. T., Ran, L., Roselle, S. J., Sarwar, G., Schwede, D. B., Sidi,



- F. I., Spero, T. L., and Wong, D. C.: The Community Multiscale Air Quality (CMAQ) model versions 5.3 and 5.3.1: system updates and evaluation, *Geosci. Model Dev.*, 14, 2867–2897, <https://doi.org/10.5194/gmd-14-2867-2021>, 2021.
- 325 Binkowski, F. S. and Roselle, S. J.: Models-3 Community Multiscale Air Quality (CMAQ) Model Aerosol Component 1. Model Description, *J. Geophys. Res. Atmos.*, 108, <https://doi.org/10.1029/2001JD001409>, 2003.
- Chang, J. C. and Hanna, S. R.: Air Quality Model Performance Evaluation, *Meteorol. Atmos. Phys.*, 87, 167–196, <https://doi.org/10.1007/s00703-003-0070-7>, 2004.
- Chang, W., Zhang, Y., Li, Z., Chen, J., and Li, K.: Improving the sectional Model for Simulating Aerosol Interactions and Chemistry (MOSAIC) aerosols of the Weather Research and Forecasting-Chemistry (WRF-Chem) model with the revised Gridpoint Statistical Interpolation system and multi-wavelength aerosol optical measurements: the dust aerosol observation campaign at Kashi, near the Taklimakan Desert, northwestern China, *Atmos. Chem. Phys.*, 21, 4403–4430, <https://doi.org/10.5194/acp-21-4403-2021>, 2021.
- 330 (MOSAIC) aerosols of the Weather Research and Forecasting-Chemistry (WRF-Chem) model with the revised Gridpoint Statistical Interpolation system and multi-wavelength aerosol optical measurements: the dust aerosol observation campaign at Kashi, near the Taklimakan Desert, northwestern China, *Atmos. Chem. Phys.*, 21, 4403–4430, <https://doi.org/10.5194/acp-21-4403-2021>, 2021.
- Chen, J.-P. and Lamb, D.: Simulation of Cloud Microphysical and Chemical Processes Using a Multicomponent Framework. Part I: Description of the Microphysical Model, *J. Atmos. Sci.*, 51, 2613 – 2630, [https://doi.org/10.1175/1520-0469\(1994\)051<2613:SOCMAC>2.0.CO;2](https://doi.org/10.1175/1520-0469(1994)051<2613:SOCMAC>2.0.CO;2), 1994.
- 335 0469(1994)051<2613:SOCMAC>2.0.CO;2, 1994.
- Debry, E. and Sportisse, B.: Solving Aerosol Coagulation with Size-Binning Methods, *Appl. Numer. Math.*, 57, 1008–1020, <https://doi.org/10.1016/j.apnum.2006.09.007>, 2007.
- Dergaoui, H., Sartelet, K. N., Debry, É., and Seigneur, C.: Modeling Coagulation of Externally Mixed Particles: Sectional Approach for Both Size and Chemical Composition, *J. Aerosol Sci.*, 58, 17–32, <https://doi.org/10.1016/j.jaerosci.2012.11.007>, 2013.
- 340 Devilliers, M., Debry, É., Sartelet, K., and Seigneur, C.: A New Algorithm to Solve Condensation/Evaporation for Ultra Fine, Fine, and Coarse Particles, *J. Aerosol Sci.*, 55, 116–136, <https://doi.org/10.1016/j.jaerosci.2012.08.005>, 2013.
- Fanourgakis, G. S., Kanakidou, M., Nenes, A., Bauer, S. E., Bergman, T., Carslaw, K. S., Grini, A., Hamilton, D. S., Johnson, J. S., Karydis, V. A., Kirkevåg, A., Kodros, J. K., Lohmann, U., Luo, G., Makkonen, R., Matsui, H., Neubauer, D., Pierce, J. R., Schmale, J., Stier, P., Tsigaridis, K., van Noije, T., Wang, H., Watson-Parris, D., Westervelt, D. M., Yang, Y., Yoshioka, M., Daskalakis, N., Decesari, S., Gysel-Beer, M., Kalivitis, N., Liu, X., Mahowald, N. M., Myriokefalitakis, S., Schrödner, R., Sfakianaki, M., Tsimpidi, A. P., Wu, M., and Yu, F.: Evaluation of Global Simulations of Aerosol Particle and Cloud Condensation Nuclei Number, with Implications for Cloud Droplet Formation, *Atmos. Chem. Phys.*, 19, 8591–8617, <https://doi.org/10.5194/acp-19-8591-2019>, 2019.
- 345 Gysel-Beer, M., Kalivitis, N., Liu, X., Mahowald, N. M., Myriokefalitakis, S., Schrödner, R., Sfakianaki, M., Tsimpidi, A. P., Wu, M., and Yu, F.: Evaluation of Global Simulations of Aerosol Particle and Cloud Condensation Nuclei Number, with Implications for Cloud Droplet Formation, *Atmos. Chem. Phys.*, 19, 8591–8617, <https://doi.org/10.5194/acp-19-8591-2019>, 2019.
- Fast, J. D., Gustafson Jr., W. I., Easter, R. C., Zaveri, R. A., Barnard, J. C., Chapman, E. G., Grell, G. A., and Peckham, S. E.: Evolution of Ozone, Particulates, and Aerosol Direct Radiative Forcing in the Vicinity of Houston Using a Fully Coupled Meteorology-Chemistry-Aerosol Model, *J. Geophys. Res. Atmos.*, 111, <https://doi.org/10.1029/2005JD006721>, 2006.
- 350 Aerosol Model, *J. Geophys. Res. Atmos.*, 111, <https://doi.org/10.1029/2005JD006721>, 2006.
- Fast, J. D., Gustafson Jr., W. I., Berg, L. K., Shaw, W. J., Pekour, M., Shrivastava, M., Barnard, J. C., Ferrare, R. A., Hostetler, C. A., Hair, J. A., Erickson, M., Jobson, B. T., Flowers, B., Dubey, M. K., Springston, S., Pierce, R. B., Dolislager, L., Pederson, J., and Zaveri, R. A.: Transport and Mixing Patterns over Central California during the Carbonaceous Aerosol and Radiative Effects Study (CARES), *Atmos. Chem. Phys.*, 12, 1759–1783, <https://doi.org/10.5194/acp-12-1759-2012>, 2012.
- 355 Forster, P., Storelvmo, T., Armour, K., Collins, W., Dufresne, J.-L., Frame, D., Lunt, D., Mauritsen, T., Palmer, M., Watanabe, M., Wild, M., and Zhang, H.: Chapter 7: The Earth energy budget, climate feedbacks, and climate sensitivity, <https://doi.org/10.25455/wgtn.16869671>, 2021.
- Frohn, L. M., Ketzler, M., Christensen, J. H., Brandt, J., Im, U., Massling, A., Andersen, C., Plejdrup, M. S., Nielsen, O.-K., van der Gon, H. D., Manders-Groot, A., and Raaschou-Nielsen, O.: Modelling Ultrafine Particle Number Concentrations at Address Reso-



- 360 lution in Denmark from 1979-2018 – Part 1: Regional and Urban Scale Modelling and Evaluation, *Atmos. Environ.*, 264, 118 631, <https://doi.org/10.1016/j.atmosenv.2021.118631>, 2021.
- Fuchs, N.: The Mechanics of Aerosols, *Quart. J. Roy. Meteor. Soc.*, 91, 249–249, <https://doi.org/10.1002/qj.49709138822>, 1964.
- Gelbard, F.: Modeling Multicomponent Aerosol Particle Growth By Vapor Condensation, *Aer. Sci. and Technol.*, 12, 399–412, <https://doi.org/10.1080/02786829008959355>, 1990.
- 365 Gelbard, F., Tambour, Y., and Seinfeld, J. H.: Sectional Representations for Simulating Aerosol Dynamics, *J. Colloid Interface Sci.*, 76, 541–556, [https://doi.org/10.1016/0021-9797\(80\)90394-X](https://doi.org/10.1016/0021-9797(80)90394-X), 1980.
- Jacobson, M., Kittelson, D., and Watts, W.: Enhanced Coagulation Due to Evaporation and Its Effect on Nanoparticle Evolution, *Environ. Sci. and Technol.*, 39, 9486–9492, <https://doi.org/10.1021/es0500299>, 2005.
- Jacobson, M. Z.: Development and application of a new air pollution modeling system - II. Aerosol module structure and design, *Atmos. Environ.*, 31, 131–144, [https://doi.org/10.1016/1352-2310\(96\)00202-6](https://doi.org/10.1016/1352-2310(96)00202-6), 1997.
- 370 Karl, M., Pirjola, L., Grönholm, T., Kurppa, M., Anand, S., Zhang, X., Held, A., Sander, R., Dal Maso, M., Topping, D., Jiang, S., Kangas, L., and Kukkonen, J.: Description and Evaluation of the Community Aerosol Dynamics Model MAFOR v2.0, *gmd*, 15, 3969–4026, <https://doi.org/10.5194/gmd-15-3969-2022>, 2022.
- Kokkola, H., Kühn, T., Laakso, A., Bergman, T., Lehtinen, K. E. J., Mielonen, T., Arola, A., Stadtler, S., Korhonen, H., Ferrachat, S., Lohmann, U., Neubauer, D., Tegen, I., Siegenthaler-Le Drian, C., Schultz, M. G., Bey, I., Stier, P., Daskalakis, N., Heald, C. L., and Romakkaniemi, S.: SALSA2.0: The sectional aerosol module of the aerosol–chemistry–climate model ECHAM6.3.0-HAM2.3-MOZ1.0, *Geosci. Model Dev.*, 11, 3833–3863, <https://doi.org/10.5194/gmd-11-3833-2018>, 2018.
- Kwon, H.-S., Ryu, M. H., and Carlsten, C.: Ultrafine Particles: Unique Physicochemical Properties Relevant to Health and Disease, *Exp. Mol. Med.*, 52, 318–328, <https://doi.org/10.1038/s12276-020-0405-1>, 2020.
- 380 Laaksonen, A., McGraw, R., and Vehkamäki, H.: Liquid-Drop Formalism and Free-Energy Surfaces in Binary Homogeneous Nucleation Theory, *J. Chem. Phys.*, 111, 2019–2027, <https://doi.org/10.1063/1.479470>, 1999.
- Leinonen, V., Kokkola, H., Yli-Juuti, T., Mielonen, T., Kühn, T., Nieminen, T., Heikkinen, S., Miinalainen, T., Bergman, T., Carslaw, K., Decesari, S., Fiebig, M., Hussein, T., Kivekäs, N., Krejci, R., Kulmala, M., Leskinen, A., Massling, A., Mihalopoulos, N., Mulcahy, J. P., Noe, S. M., van Noije, T., O'Connor, F. M., O'Dowd, C., Olivie, D., Pernov, J. B., Petäjä, T., Seland, Ø., Schulz, M., Scott, C. E., Skov, H., Swietlicki, E., Tuch, T., Wiedensohler, A., Virtanen, A., and Mikkonen, S.: Comparison of particle number size distribution trends in ground measurements and climate models, *Atmospheric Chemistry and Physics*, 22, 12 873–12 905, <https://doi.org/10.5194/acp-22-12873-2022>, 2022.
- Mallet, V., Quélo, D., Sportisse, B., Ahmed de Biasi, M., Debry, É., Korsakissok, I., Wu, L., Roustan, Y., Sartelet, K., Tombette, M., and Foudhil, H.: Technical Note: The Air Quality Modeling System Polyphemus, *Atmos. Chem. Phys.*, 7, 5479–5487, <https://doi.org/10.5194/acp-7-5479-2007>, 2007.
- 390 Menut, L., Bessagnet, B., Briant, R., Cholakian, A., Couvidat, F., Mailler, S., Pennel, R., Siour, G., Tuccella, P., Turquety, S., and Valari, M.: The CHIMERE v2020r1 online chemistry-transport model, *Geosci. Model Dev.*, 14, 6781–6811, <https://doi.org/10.5194/gmd-14-6781-2021>, 2021.
- Neuman, S. P.: Adaptive Eulerian–Lagrangian Finite Element Method for Advection–Dispersion, *Int. J. Numer. Meth. Eng.*, 20, 321–337, <https://doi.org/10.1002/nme.1620200211>, 1984.
- 395 Ohlwein, S., Kappeler, R., Kutlar Joss, M., Künzli, N., and Hoffmann, B.: Health Effects of Ultrafine Particles: A Systematic Literature Review Update of Epidemiological Evidence, *Int. J. Public Health*, 64, 547–559, <https://doi.org/10.1007/s00038-019-01202-7>, 2019.



- Olin, M., Patoulias, D., Kuuluvainen, H., Niemi, J. V., Rönkkö, T., Pandis, S. N., Riipinen, I., and Dal Maso, M.: Contribution of Traffic-Originated Nanoparticle Emissions to Regional and Local Aerosol Levels, *Atmos. Chem. Phys.*, 22, 1131–1148, <https://doi.org/10.5194/acp-22-1131-2022>, 2022.
- Pandis, S. N., Harley, R. A., Cass, G. R., and Seinfeld, J. H.: Secondary Organic Aerosol Formation and Transport, *Atmos. Environ.*, 26, 2269–2282, [https://doi.org/10.1016/0960-1686\(92\)90358-R](https://doi.org/10.1016/0960-1686(92)90358-R), 1992.
- Patel, S., Rim, D., Sankhyan, S., Novoselac, A., and Vance, M. E.: Aerosol dynamics modeling of sub-500 nm particles during the HOME-Chem study, *Environ. Sci.: Processes Impacts*, 23, 1706–1717, <https://doi.org/10.1039/D1EM00259G>, 2021.
- Patoulias, D., Fountoukis, C., Riipinen, I., Asmi, A., Kulmala, M., and Pandis, S. N.: Simulation of the Size-Composition Distribution of Atmospheric Nanoparticles over Europe, *Atmos. Chem. Phys.*, 18, 13 639–13 654, <https://doi.org/10.5194/acp-18-13639-2018>, 2018.
- Pilinis, C. and Seinfeld, J. H.: Development and Evaluation of an Eulerian Photochemical Gas-Aerosol Model, *Atmos. Environ.*, 22, 1985–2001, [https://doi.org/10.1016/0004-6981\(88\)90088-1](https://doi.org/10.1016/0004-6981(88)90088-1), 1988.
- Riccobono, F., Schobesberger, S., Scott, C. E., Dommen, J., Ortega, I. K., Rondo, L., Almeida, J., Amorim, A., Bianchi, F., Breitenlechner, M., David, A., Downard, A., Dunne, E. M., Duplissy, J., Ehrhart, S., Flagan, R. C., Franchin, A., Hansel, A., Junninen, H., Kajos, M., Keskinen, H., Kupc, A., Kürten, A., Kvashin, A. N., Laaksonen, A., Lehtipalo, K., Makhmutov, V., Mathot, S., Nieminen, T., Onnela, A., Petäjä, T., Praplan, A. P., Santos, F. D., Schallhart, S., Seinfeld, J. H., Sipilä, M., Spracklen, D. V., Stozhkov, Y., Stratmann, F., Tomé, A., Tsagkogeorgas, G., Vaattovaara, P., Viisanen, Y., Vrtala, A., Wagner, P. E., Weingartner, E., Wex, H., Wimmer, D., Carslaw, K. S., Curtius, J., Donahue, N. M., Kirkby, J., Kulmala, M., Worsnop, D. R., and Baltensperger, U.: Oxidation Products of Biogenic Emissions Contribute to Nucleation of Atmospheric Particles, *Science*, 344, 717–721, <https://doi.org/10.1126/science.1243527>, 2014.
- Sartelet, K., Zhu, S., Moukhtar, S., Andre, M., Andre, J., Gros, V., Favez, O., Brasseur, A., and Redaelli, M.: Emission of intermediate, semi and low volatile organic compounds from traffic and their impact on secondary organic aerosol concentrations over Greater Paris, *Atmos. Environ.*, 180, 126–137, <https://doi.org/10.1016/j.atmosenv.2018.02.031>, 2018.
- Sartelet, K., Couvidat, F., Wang, Z., Flageul, C., and Kim, Y.: SSH-Aerosol v1.1: A Modular Box Model to Simulate the Evolution of Primary and Secondary Aerosols, *Atmosphere*, 11, 525, <https://doi.org/10.3390/atmos11050525>, 2020.
- Sartelet, K., Kim, Y., Couvidat, F., Merkel, M., Petäjä, T., Sciare, J., and Wiedensohler, A.: Influence of Emission Size Distribution and Nucleation on Number Concentrations over Greater Paris, *Atmos. Chem. Phys.*, 22, 8579–8596, <https://doi.org/10.5194/acp-22-8579-2022>, 2022.
- Sartelet, K. N., Hayami, H., Albriet, B., and Sportisse, B.: Development and Preliminary Validation of a Modal Aerosol Model for Tropospheric Chemistry: MAM, *Aer. Sci. and Technol.*, 40, 118–127, <https://doi.org/10.1080/02786820500485948>, 2006.
- Sartelet, K. N., Hayami, H., and Sportisse, B.: Dominant Aerosol Processes during High-Pollution Episodes over Greater Tokyo, *J. Geophys. Res. Atmos.*, 112, <https://doi.org/10.1029/2006JD007885>, 2007.
- Schraufnagel, D. E.: The Health Effects of Ultrafine Particles, *Exp. Mol. Med*, 52, 311–317, <https://doi.org/10.1038/s12276-020-0403-3>, 2020.
- Seigneur, C.: A model of sulfate aerosol dynamics in atmospheric plumes, *Atmos. Environ.*, 16, 2207–2228, <https://doi.org/10.1080/02786828608959088>, 1982.
- Seigneur, C., Hudischewskyj, A. B., Seinfeld, J. H., Whitby, K. T., Whitby, E. R., Brock, J. R., and Barnes, H. M.: Simulation of Aerosol Dynamics: A Comparative Review of Mathematical Models, *Aer. Sci. and Technol.*, 5, 205–222, <https://doi.org/10.1080/02786828608959088>, 1986.



- 435 Thomson, W.: LX. On the Equilibrium of Vapour at a Curved Surface of Liquid, *London Edinburgh Philos. Mag. J. Sci.*, 42, 448–452, <https://doi.org/10.1080/14786447108640606>, 1871.
- Tolman, R. C.: The Effect of Droplet Size on Surface Tension, *J. Chem. Phys.*, 17, 333–337, <https://doi.org/10.1063/1.1747247>, 1949.
- Tsang, T. H. and Rao, A.: Comparison of Different Numerical Schemes for Condensational Growth of Aerosols, *Aer. Sci. and Technol.*, 9, 271–277, <https://doi.org/10.1080/02786828808959214>, 1988.
- 440 Tzivion, S., Feingold, G., and Levin, Z.: An Efficient Numerical Solution to the Stochastic Collection Equation, *J. Atmos. Sci.*, 44, 3139–3149, [https://doi.org/10.1175/1520-0469\(1987\)044<3139:AENSTT>2.0.CO;2](https://doi.org/10.1175/1520-0469(1987)044<3139:AENSTT>2.0.CO;2), 1987.
- v Smoluchowski, M.: Versuch einer mathematischen Theorie der Koagulationskinetik kolloider Lösungen, *Zeitschrift für Physikalische Chemie*, 92U, 129–168, <https://doi.org/10.1515/zpch-1918-9209>, 1918.
- Vehkamäki, H., Kulmala, M., Napari, I., Lehtinen, K., Timmreck, C., Noppel, M., and Laaksonen, A.: An improved parameterization for sulfuric acid-water nucleation rates for tropospheric and stratospheric conditions, *J. Geophys. Res.*, 107, 4622, <https://doi.org/10.1029/2002JD002184>, 2002.
- Vignati, E., Wilson, J., and Stier, P.: M7: An Efficient Size-Resolved Aerosol Microphysics Module for Large-Scale Aerosol Transport Models, *J. Geophys. Res. Atmos.*, 109, <https://doi.org/10.1029/2003JD004485>, 2004.
- Warren, D. R. and Seinfeld, J. H.: Simulation of Aerosol Size Distribution Evolution in Systems with Simultaneous Nucleation, Condensation, and Coagulation, *Aer. Sci. and Technol.*, 4, 31–43, <https://doi.org/10.1080/02786828508959037>, 1985.
- 450 Whitby, E., Stratmann, F., and Wilck, M.: Merging and Remapping Modes in Modal Aerosol Dynamics Models: A “Dynamic Mode Manager”, *J. Aerosol Sci.*, 33, 623–645, [https://doi.org/10.1016/S0021-8502\(01\)00197-5](https://doi.org/10.1016/S0021-8502(01)00197-5), 2002.
- Whitby, E. R. and McMurry, P. H.: Modal Aerosol Dynamics Modeling, *Aer. Sci. and Technol.*, 27, 673–688, <https://doi.org/10.1080/02786829708965504>, 1997.
- 455 Zhu, S., Sartelet, K. N., Healy, R. M., and Wenger, J. C.: Simulation of particle diversity and mixing state over Greater Paris: a model-measurement inter-comparison, *Faraday Discuss.*, 189, 547–566, <https://doi.org/10.1039/C5FD00175G>, 2016.